Supporting Information

Facile synthesis of layered $Co(OH)_2$ deposited g-C_3N_4 for activating peroxymonosulfate to degrade organic pollutants

Yingxue Zhang[a], Jianyu Qu[a], Fangjun Ding[b], Yujiao Kong[a], Xiurong Su[a,*] and Xingliang Xu[a,c]*

[a]College of Chemistry and Material Science, Shandong Agricultural University, 271018 Taian, Shandong, People's Republic of China.

[b]Shandong Agricultural University Fertilizer Sci & Tec Co., Ltd.

271600 Taian, Shandong, People's Republic of China.

[c] Foshan (Southern China) Institute for New Materials, Foshan 528200, Guangdong, China.

*Corresponding author: Xiurong Su: xrsu@sdau.edu.cn

Xingliang Xu: xxlsdau@163.com

No.	Details	Page
1	**Figure S1.** N_2 sorption isotherms curve of g-C_3N_4, $Co(OH)_2$ and $Co(OH)_2$/ g-C_3N_4.	3
2	**Table S1.** BET surface area and pore volume of g-C_3N_4, $Co(OH)_2$ and $Co(OH)_2$/ g-C_3N_4.	3
3	**Figure S2.** Zeta potential of g-C_3N_4, $Co(OH)_2$ and $Co(OH)_2$/ g-C_3N_4 at different pH.	4
4	**Figure S3.** The electrochemical impedance spectroscopy of g-C_3N_4, $Co(OH)_2$, and $Co(OH)_2$/ g-C_3N_4.	4
5	**Figure S4.** (a) The RhB removal efficiency and (b) Kinetic constants of RhB removal in different systems.	5
6	**Figure S5.** Residual PMS during the reaction system.	5
7	**Figure S6.** Kinetic curves of RhB removal at different reaction conditions. (a) PMS dosage, (b) $Co(OH)_2$/g-C_3N_4 dosage, (c) initial pH value, (d) initial concentration on RhB removal.	6
8	**Figure S7.** The TOC removal effect of $Co(OH)_2$/g-C_3N_4 over time on RhB.	7
9	**Figure S8.** (a) The RhB removal efficiency and (b) Kinetic constants of RhB removal in the different initial RhB concentration.	7
10	**Figure S9.** The degradation of various emerging organic pollutants.	8
11	**Figure S10.** Degradation efficiency of RhB after 3 cycles.	8
12	**Figure S11.** The XRD of $Co(OH)_2$/g-C_3N_4 after using PMS activation.	9
13	**Figure S12.** XPS of Co 2p for $Co(OH)_2$/g-C_3N_4 after using PMS activation.	9
14	**Figure S13.** The extracted ion chromatography(EIC) of phthalic acid.	10
15	**Figure S14.** The mass spectrogram of phthalic acid.	10
16	**Figure S15.** The extracted ion chromatography (EIC) of phthalic acid.	11
17	**Figure S16.** The mass spectrogram of phthalic acid.	11
18	**Figure S17.** The intermediates obtained by liquid mass spectrometry.	12
19	**Table S2.** Comparison of $Co(OH)_2$/g-C_3N_4 with other published materials for PMS activation.	12

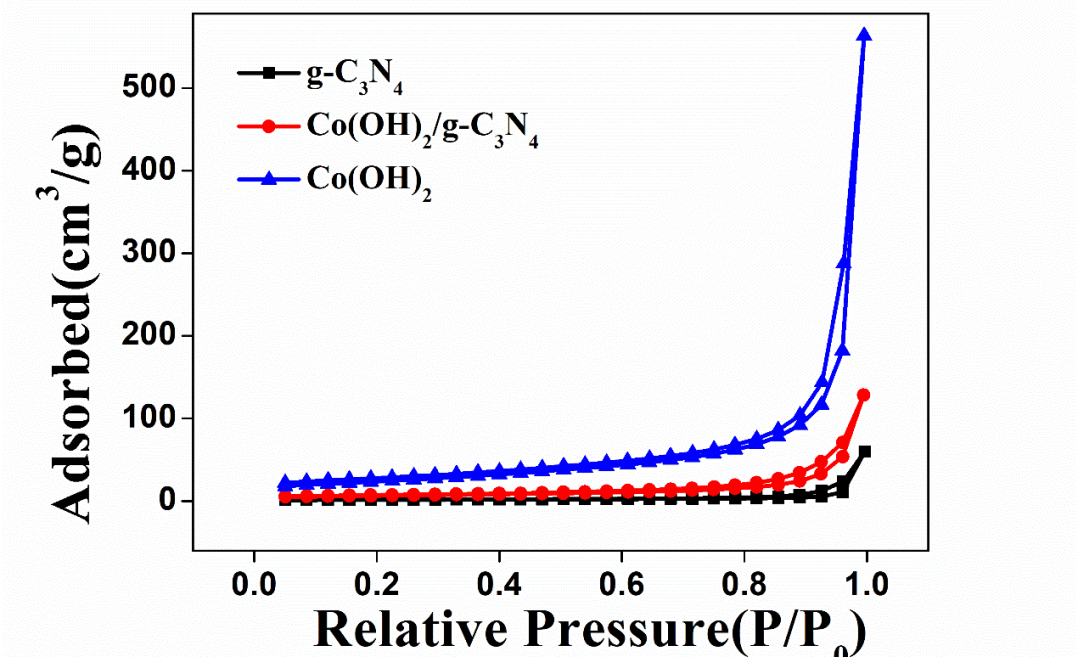

Figure S1. N_2 sorption isotherms curve of g-C_3N_4, $Co(OH)_2$ and $Co(OH)_2$/ g-C_3N_4

Table S1. BET surface area and pore volume of g-C_3N_4, $Co(OH)_2$ and $Co(OH)_2$/ g-C_3N_4.

Catalyst	S_{BET}（m^2/g）	pore volum（cm^3/g）
$Co(OH)_2$	85.5085	0.170488
g-C_3N_4	5.1232	0.013123
$Co(OH)_2$/g-C_3N_4	22.8336	0.057799

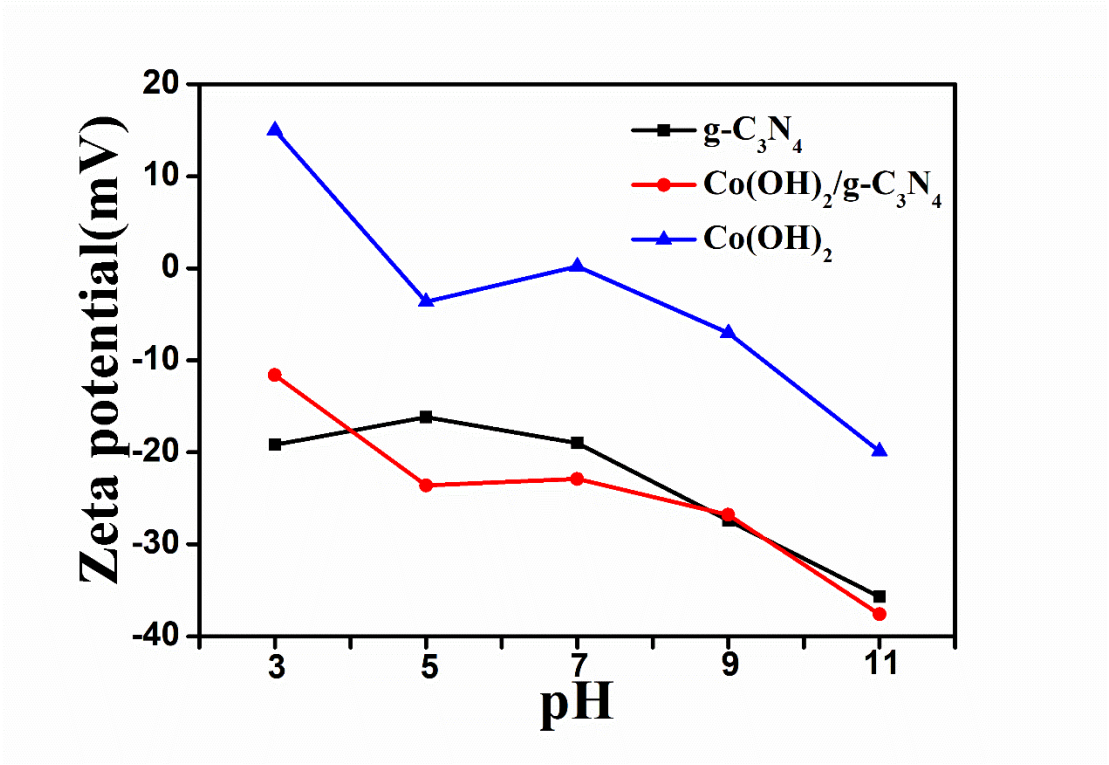

Figure S2. Zeta potential of g-C_3N_4, $Co(OH)_2$ and $Co(OH)_2$/ g-C_3N_4 at different pH.

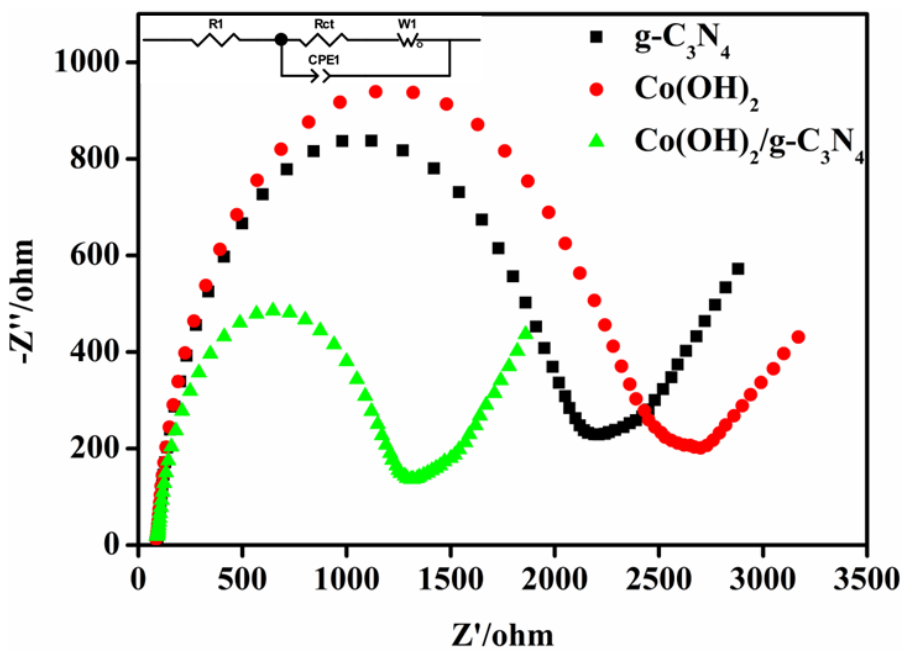

Figure S3. The electrochemical impedance spectroscopy of g-C_3N_4, $Co(OH)_2$, and $Co(OH)_2$/ g-C_3N_4.

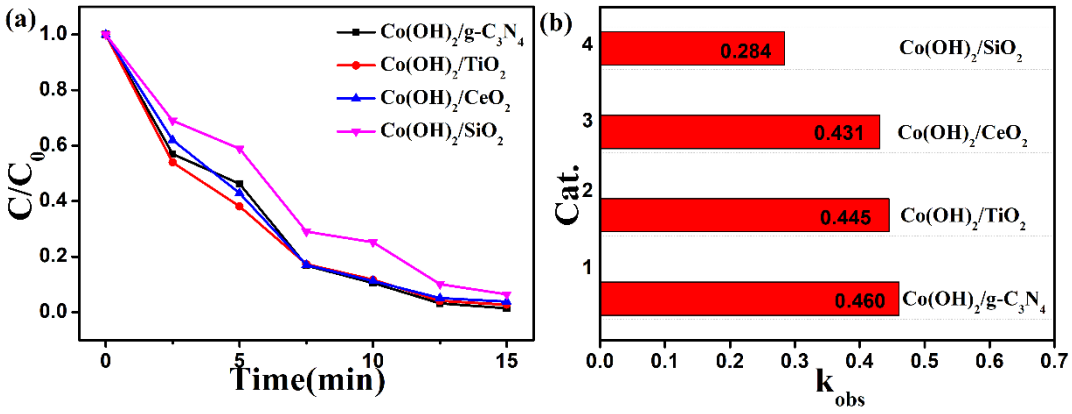

Figure S4. (a) The RhB removal efficiency and (b) Kinetic constants of RhB removal in different systems. Reaction conditions: V=100mL, $[RhB]_0$ = 20.0 mg/L, $[Cat.]_0$ = 0.15 g/L, $[PMS]_0$ = 0.50 g/L, initial pH = 7.

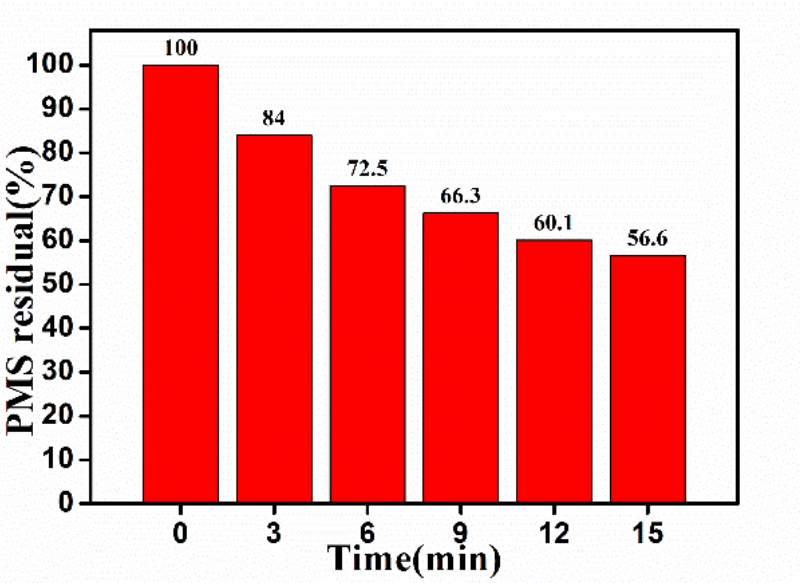

Figure S5. Residual PMS during the reaction system. Reaction conditions: V=100mL, [RhB]0 = 20.0 mg/L, [Cat.]0 = 0.15 g/L, [PMS]0 = 0.50 g/L, initial pH = 7.

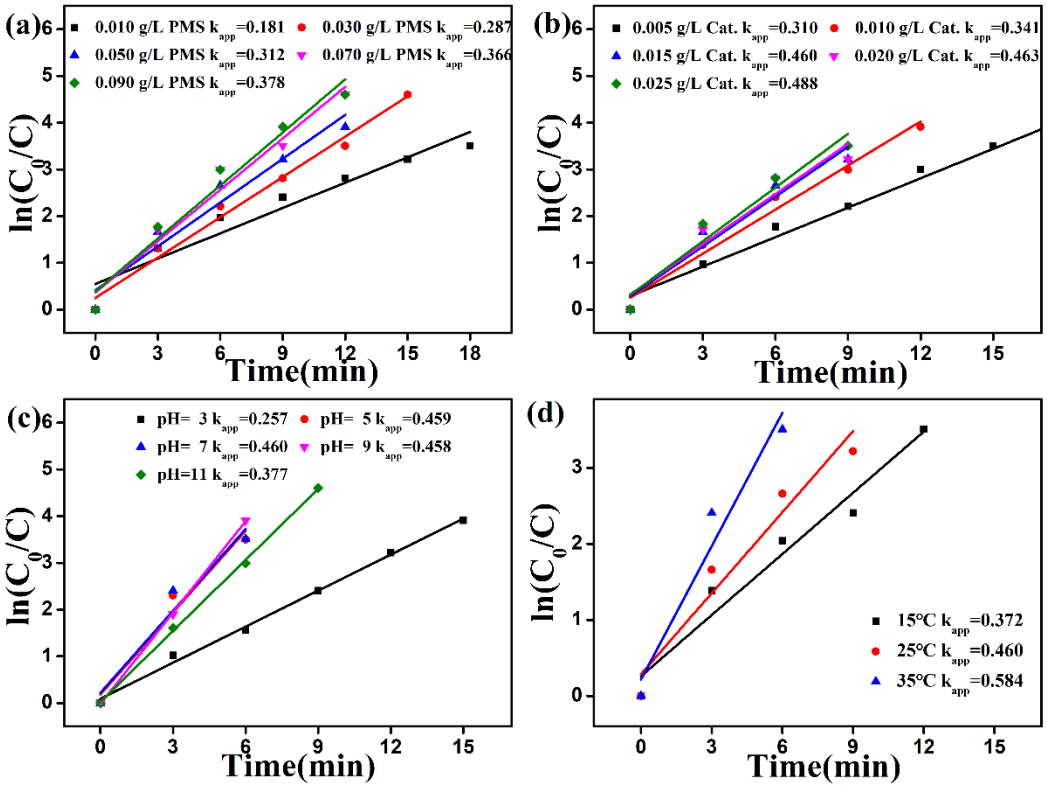

Figure S6. Kinetic curves of RhB removal at different reaction conditions.(a) PMS dosage, (b) $Co(OH)_2$/ g-C_3N_4 dosage, (c) initial pH value, (d) reaction temperature. Reaction conditions: V=100mL, $[RhB]_0$ = 20.0 mg/L, $[Co(OH)_2$/ g-$C_3N_4]_0$ = 0.15 g/L (except (a)), $[PMS]_0$ = 0.50 g/L (except (b)), initial pH = 7 (except (c)).

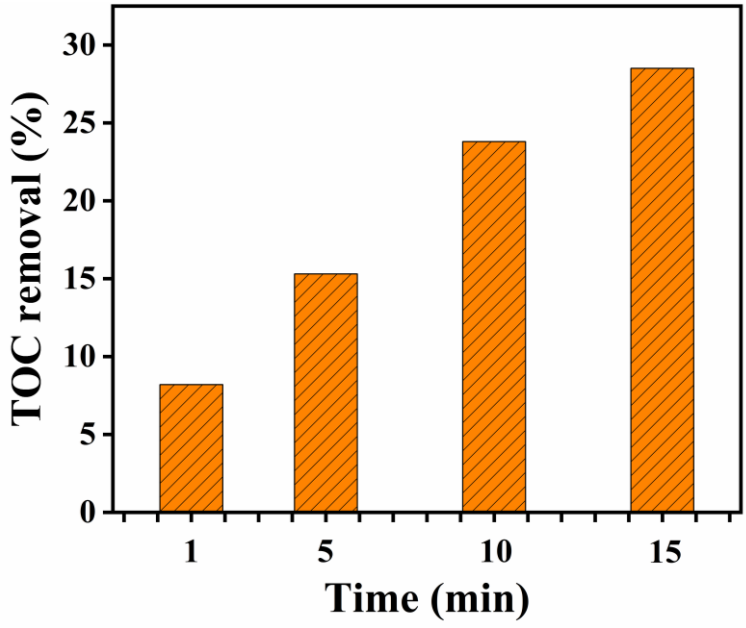

Figure S7.The TOC removal effect of $Co(OH)_2$/g-C_3N_4 over time on RhB. Reaction conditions: V = 100 mL, $[RhB]_0$ = 20.0 mg/L, $[Co(OH)_2/g\text{-}C_3N_4]_0$ = 0.15 g/L , $[PMS]_0$ = 0.50 g/L , initial pH = 7.0 .

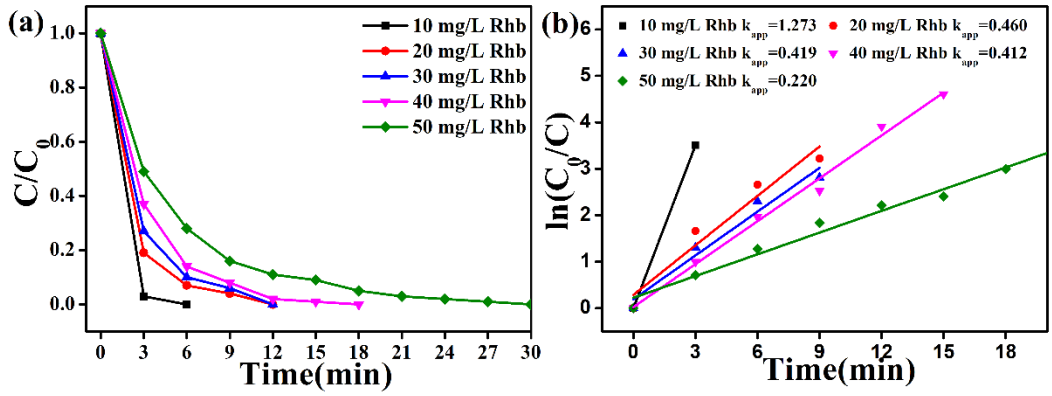

Figure S8. (a) The RhB removal efficiency and (b) Kinetic constants of RhB removal in the different initial RhB concentration. Reaction conditions: [Co(OH)2/g-C3N4]0 =0.15g/L, [PMS]0 =0.5g/L, initial pH =7.

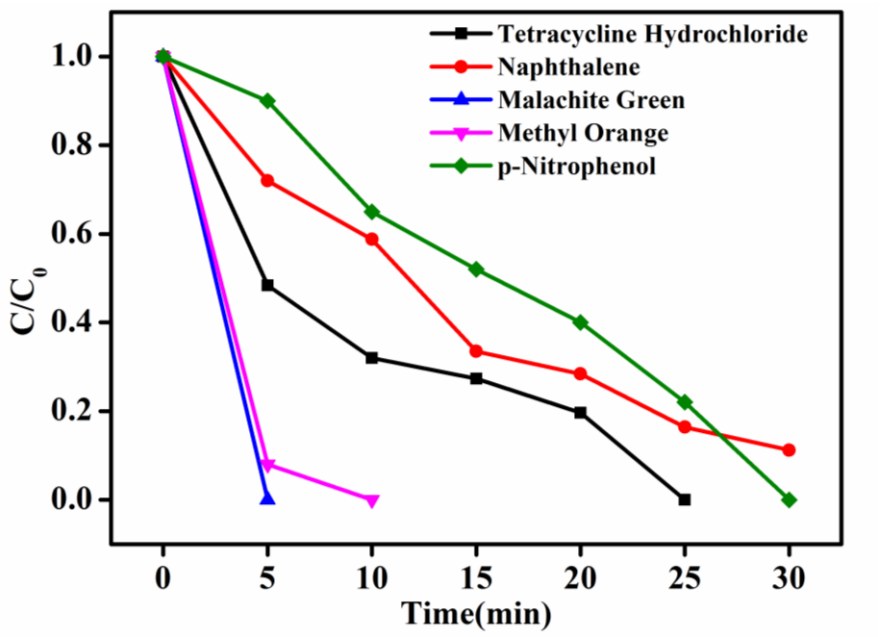

Figure S9. The degradation of various emerging organic pollutants. Reaction conditions: V = 100 mL, [organic compounds]$_0$ = 20.0 mg/L, [Co(OH)$_2$/g-C$_3$N$_4$]$_0$ = 0.15 g/L, [PMS]$_0$ = 0.5 0g/L, initial pH = 7.0.

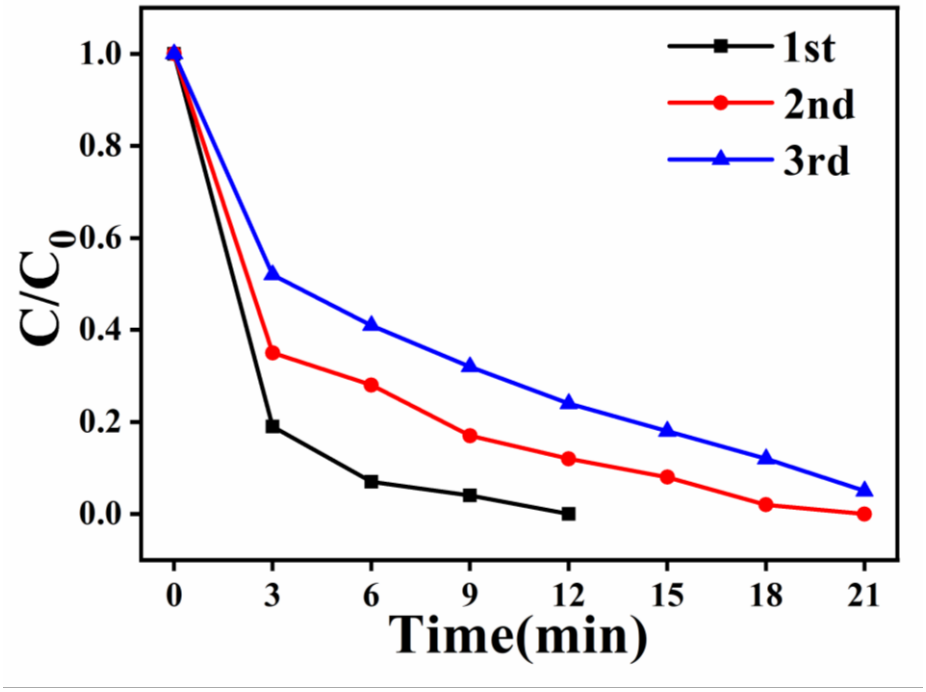

Figure S10. Degradation efficiency of RhB after 3 cycles. Reaction conditions: V=100 mL, [organic compounds]$_0$ =20.0mg/L, [Co(OH)$_2$/g-C$_3$N$_4$]$_0$ =0.15g/L, [PMS]$_0$ =0.5g/L, initial pH =7.

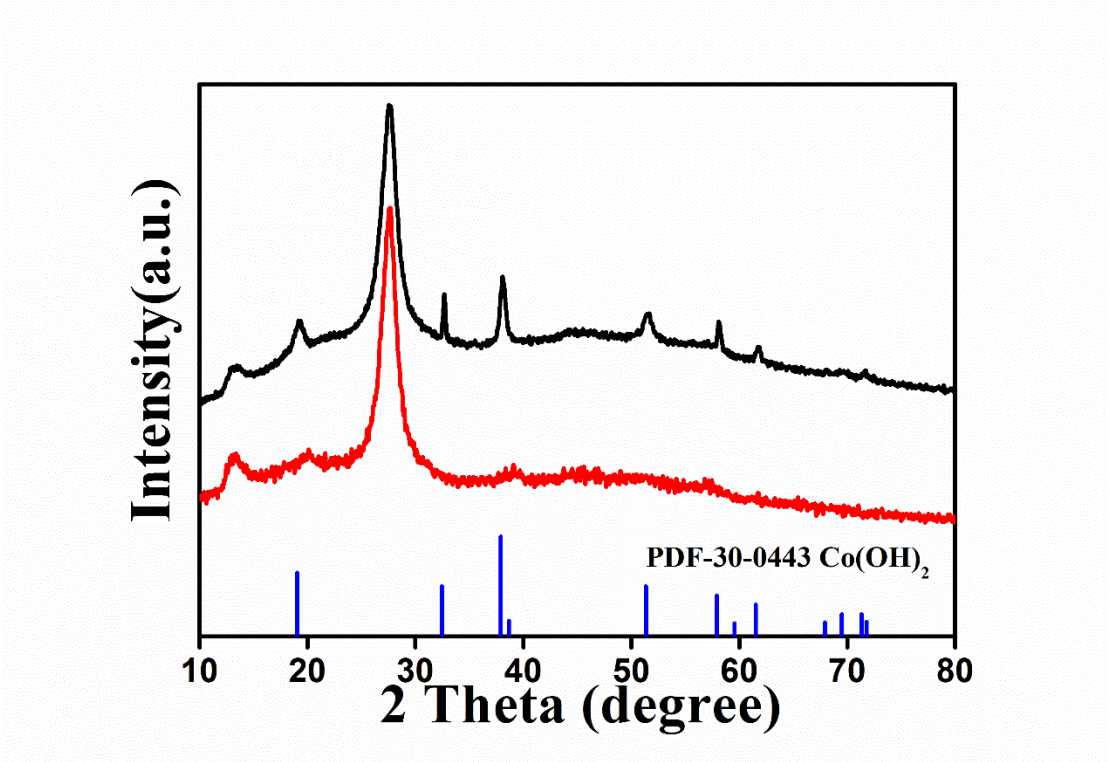

Figure S11. The XRD of $Co(OH)_2$/g-C_3N_4 after using PMS activation.

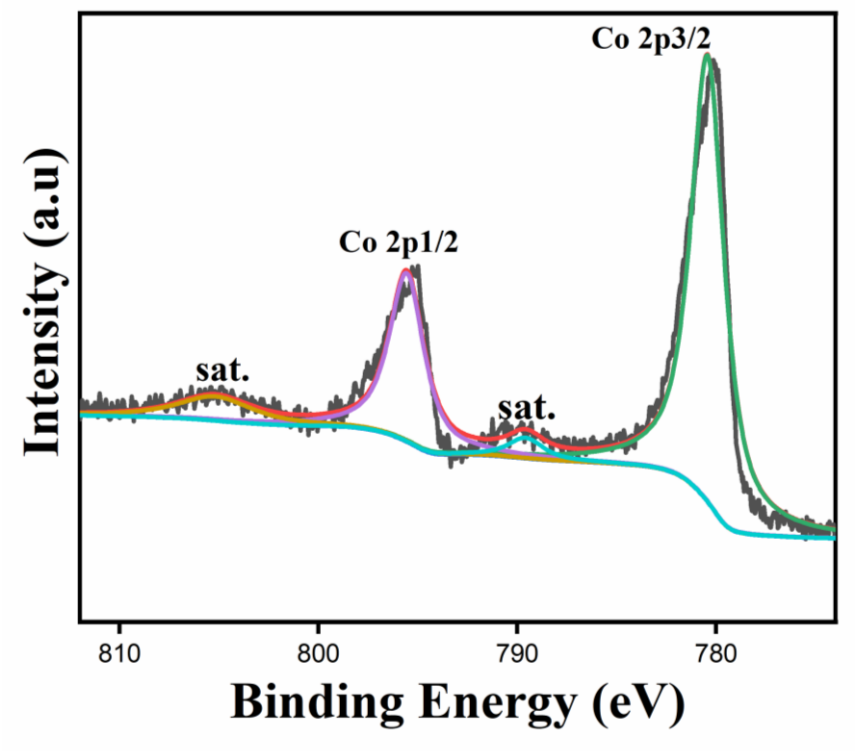

Figure S12. XPS of Co 2p for $Co(OH)_2$/g-C_3N_4 after using PMS activation.

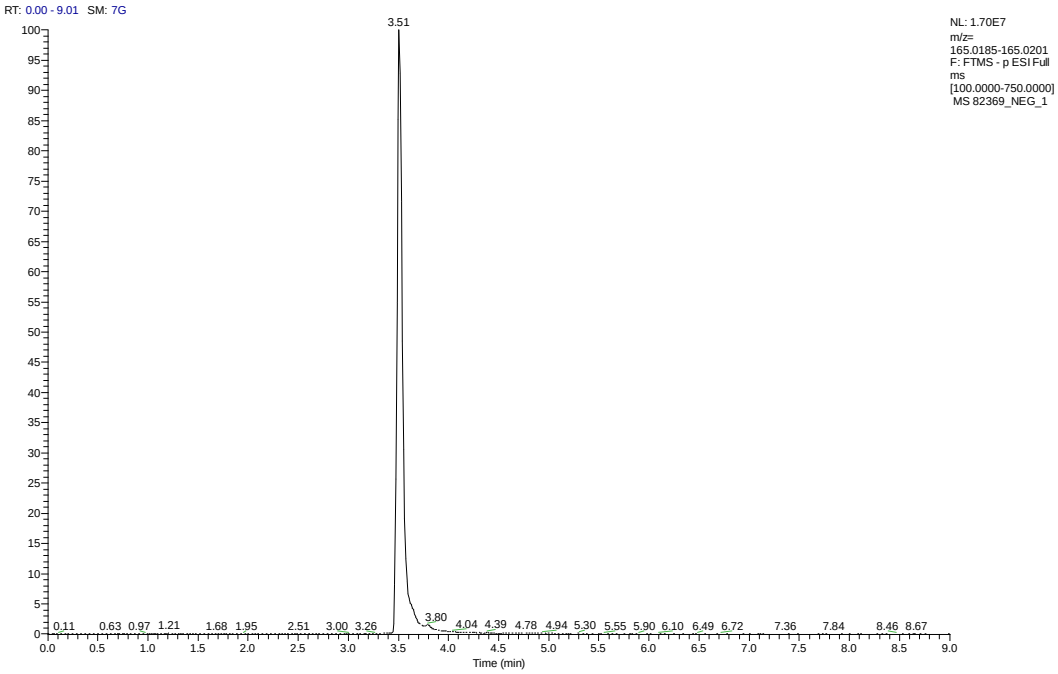

Figure S13. The extracted ion chromatography (EIC) of phthalic acid.

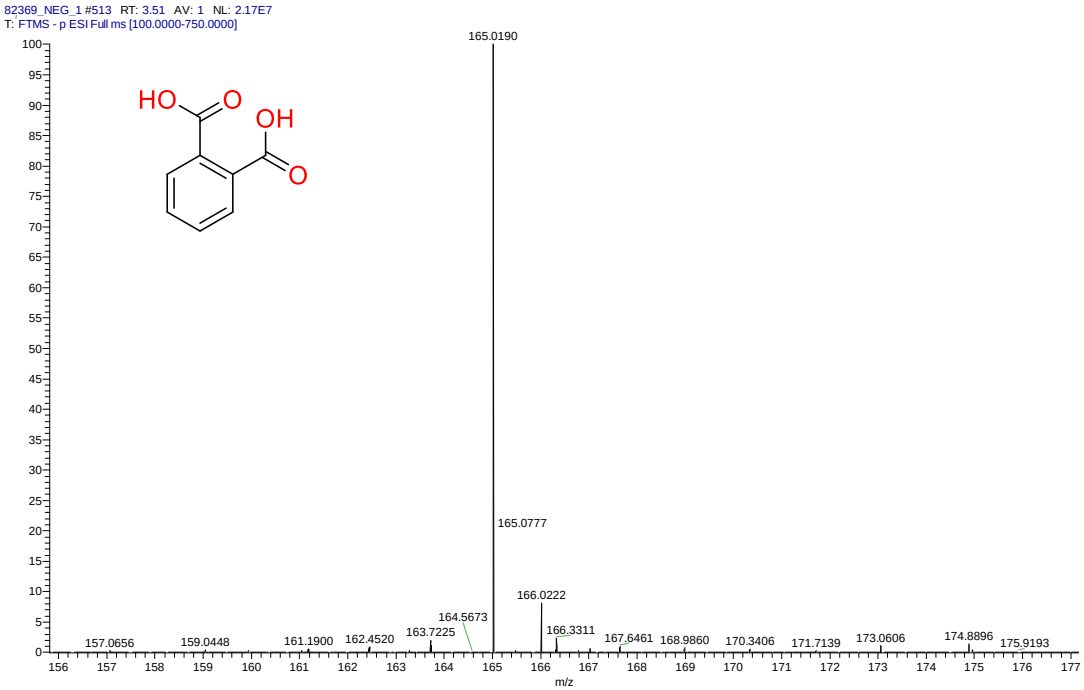

Figure S14. The mass spectrogram of phthalic acid.

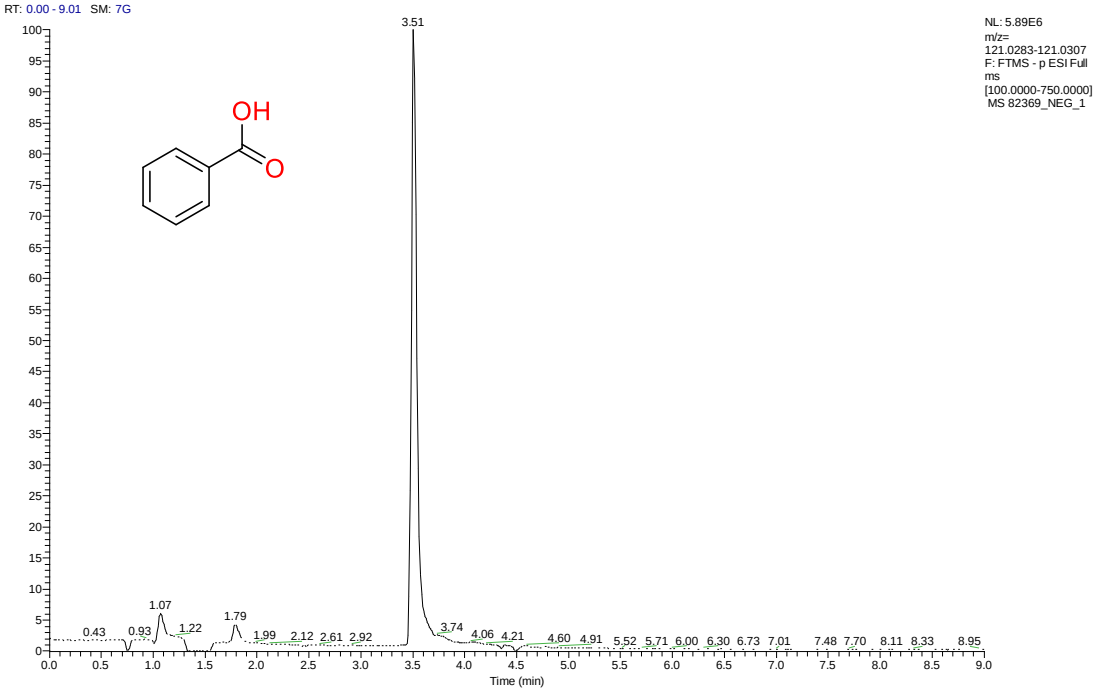

Figure S15. The extracted ion chromatography (EIC) of phthalic acid.

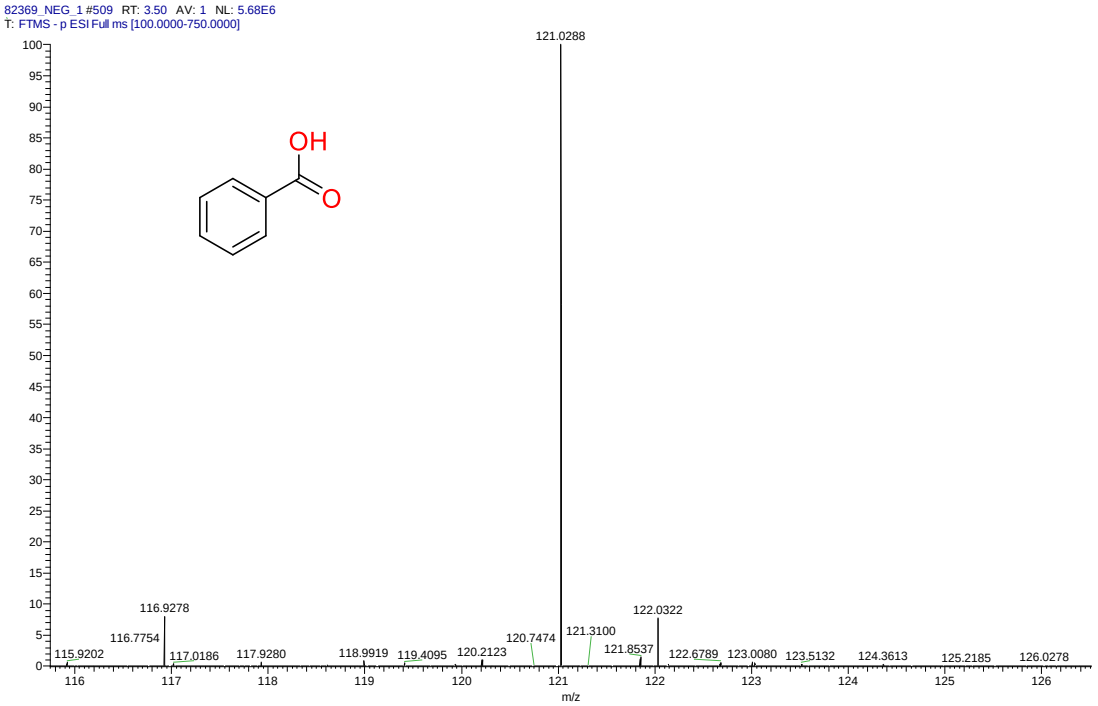

Figure S16. The mass spectrogram of phthalic acid.

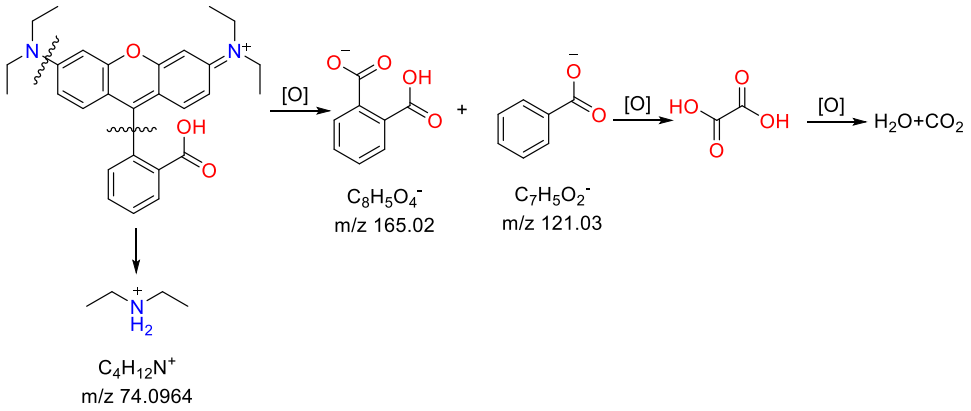

Figure S17. The intermediates obtained by liquid mass spectrometry.

Table S2. Comparison of $Co(OH)_2$/g-C_3N_4 with other published materials for PMS activation.

Contaminants		Catalyst		PMS	K_{obs}	
Type and concentration		Type and concentration		Concentration	(min^{-1})	Ref.
($g\ L^{-1}$)		($g\ L^{-1}$)				
RhB	0.1	$CoFe_2O_4$/TNTs	0.20	4.0 $g\ L^{-1}$	0.0673	[1]
RhB	0.1	$CoFe_2O_4$/OMC	0.05	1.5 mM	0.0452	[2]
RhB	0.05	$CoFe_2O_4$/diatomite	0.03	1.5 mM	0.572	[3]
RhB	0.01	Mn_3O_4/ ZIF-8	0.40	0.3 $g\ L^{-1}$	0.913	[4]
MB	0.02	$FeCo_2$@ APCFs	0.10	0.5 $g\ L^{-1}$	0.422	[5]
MB	0.02	$MnFe_2O_4$-rGO	0.05	0.5 $g\ L^{-1}$	0.019	[6]
MB	0.02	$MnFe_2O_4$	0.05	0.5 $g\ L^{-1}$	0.012	[6]
MB	**0.02**	**$Co(OH)_2$/g-C_3N_4**	**0.15**	**0.5 $g\ L^{-1}$**	**0.524**	**This work**
RhB	**0.02**	**$Co(OH)_2$/g-C_3N_4**	**0.15**	**0.5 $g\ L^{-1}$**	**0.460**	**This work**

Reference

[1] Y. Du, W. Ma, P. Liu, B. Zou, J. Ma, Magnetic $CoFe_2O_4$ nanoparticles supported on titanate nanotubes ($CoFe_2O_4$/TNTs) as a novel heterogeneous catalyst for peroxymonosulfate activation and degradation of organic pollutants, J Hazard Mater, 308 (2016) 58-66.

[2] J. Deng, Y.J. Chen, Y.A. Lu, X.Y. Ma, S.F. Feng, N. Gao, J. Li, Synthesis of

magnetic $CoFe_2O_4$/ordered mesoporous carbon nanocomposites and application in Fenton-like oxidation of rhodamine B, Environ Sci Pollut Res Int, 24 (2017) 14396-14408.

[3] Y. Wang, Y. Zhang, J. Wang, Nano spinel $CoFe_2O_4$ deposited diatomite catalytic separation membrane for efficiently cleaning wastewater, Journal of Membrane Science, 615 (2020).

[4] L. Hu, G. Deng, W. Lu, Y. Lu, Y. Zhang, Peroxymonosulfate activation by Mn_3O_4/metal-organic framework for degradation of refractory aqueous organic pollutant rhodamine B, Chinese Journal of Catalysis, 38 (2017) 1360-1372.

[5] Z. Zhu, C. Ji, L. Zhong, S. Liu, F. Cui, H. Sun, W. Wang, Magnetic Fe–Co crystal doped hierarchical porous carbon fibers for removal of organic pollutants, Journal of Materials Chemistry A, 5 (2017) 18071-18080.

[6] Y. Yao, Y. Cai, F. Lu, F. Wei, X. Wang, S. Wang, Magnetic recoverable $MnFe_2O_4$ and $MnFe_2O_4$-graphene hybrid as heterogeneous catalysts of peroxymonosulfate activation for efficient degradation of aqueous organic pollutants, J Hazard Mater, 270 (2014) 61-70.